Article

Controlled Synthesis and Upconverted Avalanche Luminescence of Cerium(III) and Neodymium(III) Orthovanadate Nanocrystals with High Uniformity of Size and Shape

Hong Deng, Shihe Yang, Si Xiao, Hong-Mei Gong, and Qu-Quan Wang

J. Am. Chem. Soc., **2008**, 130 (6), 2032-2040 • DOI: 10.1021/ja0778141

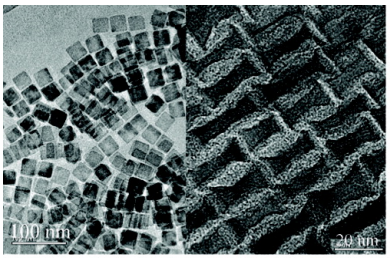

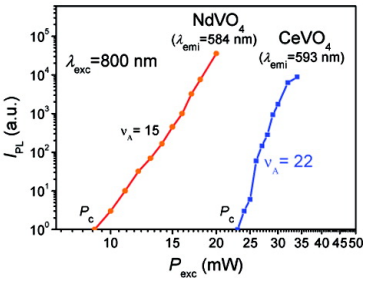

More About This Article

Additional resources and features associated with this article are available within the HTML version:

- Supporting Information
- Links to the 3 articles that cite this article, as of the time of this article download
- Access to high resolution figures
- Links to articles and content related to this article
- Copyright permission to reproduce figures and/or text from this article

View the Full Text HTML

J|A|C|S
ARTICLES
Published on Web 01/17/2008

Controlled Synthesis and Upconverted Avalanche Luminescence of Cerium(III) and Neodymium(III) Orthovanadate Nanocrystals with High Uniformity of Size and Shape

Hong Deng,[†] Shihe Yang,*[,†] Si Xiao,[‡] Hong-Mei Gong,[‡] and Qu-Quan Wang*[,‡]

Department of Chemistry, The Hong Kong University of Science and Technology, Clear Water Bay, Kowloon, Hong Kong, China, and Department of Physics and Key Laboratory of Acoustic and Photonic Materials and Devices of Ministry of Education, Wuhan University, Wuhan 430072, China

Received October 11, 2007; E-mail: chsyang@ust.hk; qqwang@whu.edu.cn

Abstract: We report on controlled synthesis of uniform $LnVO_4$ (Ln = Ce and Nd) nanocrystals (NCs) with square-plate and H-shaped morphologies in nanosized reverse microemulsion reactors, via a facile solvo/hydrothermal strategy. The NCs were thoroughly characterized by X-ray diffraction, transmission electron microscopy (TEM), atomic force microscopy (AFM), energy-dispersive X-ray spectroscopy (EDS), infrared absorption spectroscopy, and photoluminescence. Possible mechanisms of the rare-earth orthovanadate NC growth and size and shape evolution are proposed. A unique upconverted avalanche luminescence property pertaining to the NCs has been discovered, systematically studied, and mechanistically discussed. Our work combines synthetic and optical studies of the NCs and lays a foundation for reinventing their applications in optoelectronics among others.

Introduction

Monodispersed nanocrystals (NCs), with reduced dimensions, exhibit novel chemical, optical, electrical, and magnetic properties not seen in their bulk counterparts, and have therefore attracted increasing research interest over the past decade for both their fundamental and technological importance.[1−4] It has been established that the properties of NCs are highly size- and shape-dependent, accentuating the necessity for the synthesis of NCs with high monodispersity and shape uniformity. Promising applications of uniform semiconductor NCs in optoelectronics, catalysis, and biomedicine have driven the development of a wide variety of strategies for their synthesis, including sol−gel techniques, coprecipitation, microemulsion, methods, ultrasound irradiation, laser pyrolysis techniques, and thermal decomposition of organometallic compounds, etc.[5−7] Our own previous work involved synthesis of semiconductor NCs assisted by hydrothermal, polymer, surfactant templates, and chemical vapor deposition.[8] However, major challenges remain for the preparation of ideal NCs, particularly rare-earth compound NCs, with well-tailored, uniform dimensionality, size and shape, high crystallinity, high dispersibility, and desired properties.

Multiphoton induced fluorescence materials are expected to have a broad range of possible applications in microfabrication,

[†] The Hong Kong University of Science and Technology.
[‡] Wuhan University.

(1) (a) Robinson, R. D.; Sadtler, B.; Demchenko, D. O.; Erdonmez, C. K.; Wang, L.; Alivisatos, A. P. *Science* **2007**, *317*, 355−358. (b) Yin, Y. D.; Alivisatos, A. P. *Nature* **2005**, *437*, 664−670. (c) Puntes, V. F.; Krishnan, K. M.; Alivisatos, A. P. *Science* **2001**, *291*, 2115−2117. (d) Peng, X. G.; Manna, L.; Yang, W. D.; Wickham, J.; Scher, E.; Kadavanich, A.; Alivisatos, A. P. *Nature* **2000**, *404*, 59−61. (e) Chen, C. C.; Herhold, A. B.; Johnson, C. S.; Alivisatos, A. P. *Science* **1997**, *276*, 398−401. (f) Yin, Y. D.; Rioux, R. M.; Erdonmez, C. K.; Hughes, S.; Somorjai, G. A.; Alivisatos, A. P. *Science* **2004**, 711−714.
(2) (a) Wang, X.; Zhuang, J.; Peng, Q.; Li, Y. D. *Nature* **2005**, *437*, 121−124. (b) Wang, X.; Peng, Q.; Li, Y. D. *Acc. Chem. Res.* **2007**, *40*, 635−643. (c) Deng, H.; Li, X. L.; Peng, Q.; Wang, X.; Chen, J. P.; Li, Y. D. *Angew. Chem., Int. Ed.* **2005**, *44*, 2782−2785. (d) Wang, X.; Zhuang, J.; Peng, Q.; Li, Y. D. *Adv. Mater.* **2006**, *18*, 2031−2034.
(3) (a) Sun, Y.; Xia, Y. N. *Science* **2002**, *298*, 2176−2179. (b) Wiley, B.; Sun, Y.; Mayers, B.; Xia, Y. N. *Chem. Eur. J.* **2005**, *11*, 454−463. (c) Jin, R.; Cao, Y.; Mirkin, C. A.; Kelly, K. L.; Schatz, G. C.; Zheng, J. G. *Science* **2001**, *294*, 1901−1904. (d) Park, J.; Joo, J.; Kwon, S. G.; Jang, Y.; Hyeon, T. *Angew. Chem., Int. Ed.* **2007**, *46*, 4630−4660.
(4) (a) Sun, S. H.; Murray, C. B.; Weller, D.; Folks, L.; Moser, A. *Science* **2000**, *287*, 1989−1992. (b) Zeng, H.; Li, J.; Zhong, L.; Sun, S. *Nature* **2002**, *420*, 395−398. (c) Chan, W. C. W.; Ni, S. M. *Science* **1998**, *281*, 2016−2018. (d) Hyeon, T. *Chem. Com.* **2003**, 927−934. (e) Hyeon, T.; Lee, S. S.; Park, J.; Chung, Y.; Na, H. B. *J. Am. Chem. Soc.* **2001**, *123*, 12789−127. (f) Guo, L.; Yang, S. H.; Yang, C. L.; Yu, P.; Wang, J. N.; Ge, W. K.; Wong, G. K. L. *Appl. Phys. Lett.* **2000**, *76*, 2901−2903.
(5) (a) Son, D. H.; Hughes, S. M.; Yin, Y. D.; Alivisatos, A. P. *Science* **2004**, *306*, 1009−1012. (b) Matijević, E. *Acc. Chem. Res.* **1981**, *14*, 22−29. (c) Sugimoto, T. *Monodispersed Particles*; Elsevier: New York, 2001.
(6) (a) Peng, X. *Adv. Mater.* **2003**, *15*, 459−463. (b) Lu, A.; Salabas, E. L.; Schüth, F. *Angew. Chem., Int. Ed.* **2007**, *46*, 1222−1244. (c) El-Sayed, M. A. *Acc. Chem. Res.* **2004**, *37*, 326−333. (d) Duan, X. F.; Huang, Y.; Cui, Y.; Wang, J. F.; Lieber, C. M. *Nature* **2001**, *409*, 66−69. (e) Hu, J. T.; Odom, T. W.; Lieber, C. M. *Acc. Chem. Res.* **1999**, *32*, 435−445.
(7) (a) Sun, S.; Zeng, H. *J. Am. Chem. Soc.* **2002**, *124*, 8204−828205. (b) Kovalenko, M. V.; Bodnarchuk, M. I.; Lechner, R. T.; Hesser, G.; Schäffler, F.; Heiss, W. *J. Am. Chem. Soc.* **2007**, *129*, 6352−6353. (c) Chen, Y.; Johnson, E.; Peng, X. *J. Am. Chem. Soc.* **2007**, *129*, 10937−10947. (d) Parkinson, B. A.; Nath, M. *Adv. Mater.* **2006**, *18*, 1865−1868.
(8) (a) Fang, Y. P.; Yang, S. H. *Angew. Chem., Int. Ed.* **2005**, *44*, 3562−3565. (b) Fang, Y. P.; Pang, Q.; Wen, X. G.; Wang, J. N.; Yang, S. H. *Small* **2006**, *2*, 612−615. (c) Zeng, Z. H.; Wang, S. H.; Yang, S. H. *Chem. Mater.* **1999**, *11*, 3365−3369. (d) Guo, L.; Yang, S. H.; Yang, C. L.; Yu, P.; Wang, J. N.; Ge, W. K.; Wong, G. K. L. *Chem. Mater.* **2000**, *12*, 2268−2274. (e) Wen, X. G.; Fang, Y. P.; Yang, S. H. *Angew. Chem., Int. Ed.* **2005**, *44*, 3562−3565. (f) Wen, X. G.; Yang, S. H. *Nano Lett.* **2002**, *2*, 451−454. (g) Qiu, Y. F.; Liu, D. F.; Yang, J. H.; Yang, S. H. *Adv. Mater.* **2006**, *18*, 2604−2608. (h) Qiu, Y. F.; Yang, S. H. *Adv. Funct. Mater.* **2007**, *17*, 1345−1352.

 10.1021/ja0778141 CCC: $40.75

up-conversion lasing, especially in the growing field of biomedical imaging.[9−14] Fluorescence based on molecular multiphoton absorption uses extremely brief (<1 picosecond) pulses of light to "see" directly into living tissues, to a greater depth and with less phototoxicity than other conventional imaging methods such as reverse saturable absorption, induced refraction, or scattering, etc.[15] Morphological and fluorescence quantification have been demonstrated from multiphoton imaging of endogenous fluorophores to distinguish cancerous and precancerous from normal tissues as deep as 40 μm.[16] Current chromophores are largely based on organic (such as rhodamine B) and polymeric compounds, which generally exhibit large two-photon absorption cross-section values, but are disadvantageous in their photochemical and photophysical stabilities.[12] Recent studies have focused on the multiphoton properties of inorganic materials, such as II−VI semiconductor quantum dots which offer much larger two-photon absorption cross-section values than organic fluorophores.[17] However, the II−VI semiconductors such as CdSe are eclipsed by high toxicity, and have raised serious health and environment concerns. Therefore, the search for new, promising multiphoton fluorescence nanomaterials carries on and has become ever more urgent. Nanoscale lanthanide compounds appear to be an ideal candidate for efficient multiphoton fluorescence as their bulk form is already a traditional phosphor widely used in flat-panel display, electroluminescent, and up-conversion materials.[18] For example, lanthanide orthovanadates have been widely used in catalysts, polarizers, laser host materials, and phosphor.[19]

More generally, lanthanide compound NCs are currently under vigorous investigation as next generation of catalysts, solar cells, magnetic and optoelectronic nanodevices, and biochemical labels.[18−22] Although impressive progress has been made in the research on lanthanide compound NCs, it is still challenging to synthesize these NCs with controllable size and shape, and new properties of the NCs, both intrinsic and collective, are yet to be discovered. In this paper, we report on our successful synthesis of uniform $LnVO_4$ (Ln = Ce, Nd) NCs with tunable shapes from square-plate to H-like using nanosized reverse microemulsion reactors coupled with simple solvo/hydrothermal treatments. We have uncovered and studied an unusual upconverted avalanche luminescence property of the cerium(III) and neodymium(III) orthovanadate NCs. In fact, this is, to the best our knowledge, the first report on systematic studies of avalanche upconversion of any rare-earth compound NCs, which point to a new direction for facilitating their applications in optical display, ceramic lasers, and biosensors.

Experimental Section

Materials and Reagents. Cerium(III) nitrate hexahydrate (Alfa Aesar), neodymium nitrate (the Shanghai Chemical Reagent Company), oleic acid (Aldrich), oleylamine (Aldrich), and sodium orthovanadate (Sigma) were used as received without further purification. Other chemicals were of analytical grade and used as received without further purification.

Synthesis of $LnVO_4$ (Ln = Ce, Nd) NCs. In a typical synthesis, 1 mmol $Ln(NO_3)_3{\cdot}6H_2O$ (Ln = Ce, Nd) was dissolved in 3 mL of H_2O, and the aqueous solution was added to a separately prepared solution containing 20 mL of l-octadecene, 10 mL of oleic acid and 1 mL of oleylamine. After it was stirred vigorously for 10 min, the mixture was sealed in a Teflon-lined stainless-steel autoclave of 50 mL capacity, kept at 100 °C for 0.5 h, and then allowed to cool down to room temperature. Then 1 mmol Na_3VO_4 and an appropriate amount of NaOH (depending on the desired nanocrystal shape), after dissolving in 3 mL of H_2O, were added rapidly into the above solution under vigorous stirring, and the stirring was kept for 30 min. Afterward, the mixture was sealed again in the 50 mL Teflon-lined stainless steel autoclave and maintained at 180 °C for 16−24 h.

After the autoclave was cooled down to room-temperature naturally, an excess ethanol was poured into the turbid suspension inside the autoclave. The mixture was centrifugally separated and the precipitate was collected. The as-precipitated product was washed several times with anhydrous ethanol and dried at 60 °C for 4 h.

Characterization. The as-prepared products were characterized by transmission electron microscopy (TEM), high-resolution TEM (HR-TEM), and energy-dispersive X-ray spectroscopy (EDS) using JEOL 2010F or JEOL 2010 microscopes with an accelerating voltage of 200 kV. Sample for TEM measurements were prepared by sonicating the precipitate products in toluene for 15 min and evaporating a drop of the suspension onto a carbon-coated, holey film supported on a copper grid. The heights of as-synthesized NCs were analyzed with an atomic force microscope (AFM) (Veeco, Nanoscope IIIa, Dimension). Powder X-ray diffraction (XRD) analyses were performed on a Philips PW-1830 X-ray diffractometer with Cu Kα irradiation (λ = 1.5406 Å) at a scanning speed of 0.025°/sec over the 2θ range of 20−70°. Fourier transform infrared spectroscopic (FTIR) analysis was carried out using pressed KBr disks in the region of 4000−400 cm^{-1} by using a Perkin Elmer spectrometer instrument.

Optical Measurements. The excitation source for the photoluminescence of the $LnVO_4$ films was a Ti:Sapphire CW laser (Mira 900, Coherent) with tunable wavelength in the range 700∼920 nm. A long-wavelength pass filter (LWPF) and a tunable neutral density filter (NDF) were used to filter the short wavelength noise from the laser and adjust

(9) Wang, H.; Huff, T. B.; Zweifel, D. A.; He, W.; Low, P. S.; Wei, A.; Cheng, J. X. *Proc. Natl. Acad. Sci. U.S.A.* **2005**, *102*, 15752−15756.
(10) Larson, D. R.; Zipfel, W. R.; William, R. M.; Clark, S. W.; Bruchez, M. P.; Wise, F. W.; Webb, W. W. *Science* **2003**, *300*, 1434−1436.
(11) Cumpston, B. H.; Ananthavel, S. P.; Barlow, S.; Dyer, D. L.; Ehrlich, J. E.; Erskine, L. L.; Heikal, A. A.; Kuebler, S. M.; Lee, I.-Y. S.; McCord-Maughon, D.; Qin, J.; Röckel, H.; Rumi, M.; Wu, X.-L.; Marder, S. R.; Perry, J. W. *Nature* **1999**, *398*, 51−54.
(12) Albota, M.; Beljonne, D.; Brédas, J. L.; Ehrlich, J. E.; Fu, J. Y.; Heikal, A. A.; Hess, S. E.; Kogej, T.; Levin, M. D.; Marder, S. R.; McCord-Maughon, D.; Perry, J. W.; Röckel, H.; Rumi, M.; Subramaniam, G.; Webb, W. W.; Wu, X. L.; Xu, C. *Science* **1998**, *281*, 1653−1656.
(13) Kawata, S.; Sun, H. B.; Tanaka, T.; Takada, K. *Nature* **2001**, *412*, 697−698.
(14) Kawata, S.; Kawata, Y. *Chem. Rev.* **2000**, *100*, 1777−1788.
(15) Cahalan, M. D.; Parker, I.; Wei, S. H.; Miller M. J. *Nat. Rev. Immunol.* **2002**, *2* (11), 872−880.
(16) Skala, M. C.; Squirrell, J. M.; Vrotsos, K. M.; Eickhoff, J. C.; Gendron-itzpatrick, A.; Eliceiri, K. W.; Ramanujam, N. *Cancer Res.* **2005**, *65*, 1180−1186.
(17) Pu, S. C.; Yang, M. J.; Hsu, C. C.; Lai, C. M.; Hsieh, C. C.; Lin, S. H.; Cheng, Y. M.; Chou, P. T. *Small* **2006**, *2*, 1308−1313.
(18) (a) Fang, Y. P.; Xu, A. W.; Song, R. Q.; Zhang, H. X.; You, L. P.; Yu, J. C.; Liu, H. Q. *J. Am. Chem. Soc.* **2003**, *125*, 16025−16034. (b) Wang, X.; Li, Y. D. *Angew. Chem., Int. Ed.* **2002**, *41*, 4790−4793. (c) Wang, X.; Li, Y. D. *Angew. Chem., Int. Ed.* **2003**, *42*, 3497−3500. (d) Zhang, Y. W.; Sun, X.; Si, R.; You, L. P.; Yan, C. H. *J. Am. Chem. Soc.* **2005**, *127*, 3260−3261.
(19) (a) O'Connor, J. R. *Appl. Phys. Lett.* **1966**, *9*, 407−409. (b) Fang, Z. M.; Hong, Q.; Zhou, Z. H.; Dai, S. J.; Weng, W. Z.; Wan, H. L. *Catal. Lett.* **1999**, *61*, 39−44. (c) Jia, C. J.; Sun, L. D.; Luo, F.; Jiang, X. C.; Wei, L. H.; Yan, C. H. *Appl. Phys. Lett.* **2004**, *84*, 5305−5307. (d) Liu, J. F.; Yao, Q. H.; Li, Y. D. *Appl. Phys. Lett.* **2006**, *88*, 173119. (e) Liu, J. F.; Li, Y. D. *Adv. Mater.* **2007**, *19*, 1118−1122.
(20) (a) Yan, C. H.; Sun, L. D.; Liao, C. S.; Zhang, Y. X.; Lu, Y. Q.; Huang, S. H.; Lu, S. Z. *Appl. Phys. Lett.* **2003**, *82*, 3511−3513. (b) Huignard, A.; Buissette, V.; Laurent, G.; Gacoin, T.; Boilot, J. P. *Chem. Mater.* **2002**, *14*, 2264−2269.
(21) (a) Boyer, J. C.; Cuccia, L. A.; Capobianco, J. A. *Nano Lett.* **2007**, *7*, 847−852. (b) Wang, L. Y.; Yan, R. X.; Huo, Z. Y.; Wang, L.; Zeng, J. H.; Bao, J.; Wang, X.; Peng, Q.; Li, Y. D. *Angew. Chem., Int. Ed.* **2005**, *44*, 6054−6057. (c) Sivakumar, S.; Veggel, F. C. J. M. V.; Raudsepp, M. J. *J. Am. Chem. Soc.* **2005**, *127*, 12464−12465.
(22) (a) Yam, V. W.; Li, Q. *Angew. Chem., Int. Ed.* **2007**, *46*, 3486−3489. (b) Stouwdam, J. W.; Veggel, F. C. J. M. van *Nano Lett.* **2002**, *2*, 733−737. (c) Bender, C. M.; Burlitch, J. M. *Chem. Mater.* **2000**, *12*, 1969−1976. (d) Yada, M.; Mihara, M.; Mouri, S.; Kuroki, M.; Kijima, T. *Adv. Mater.* **2000**, *12*, 309−313.

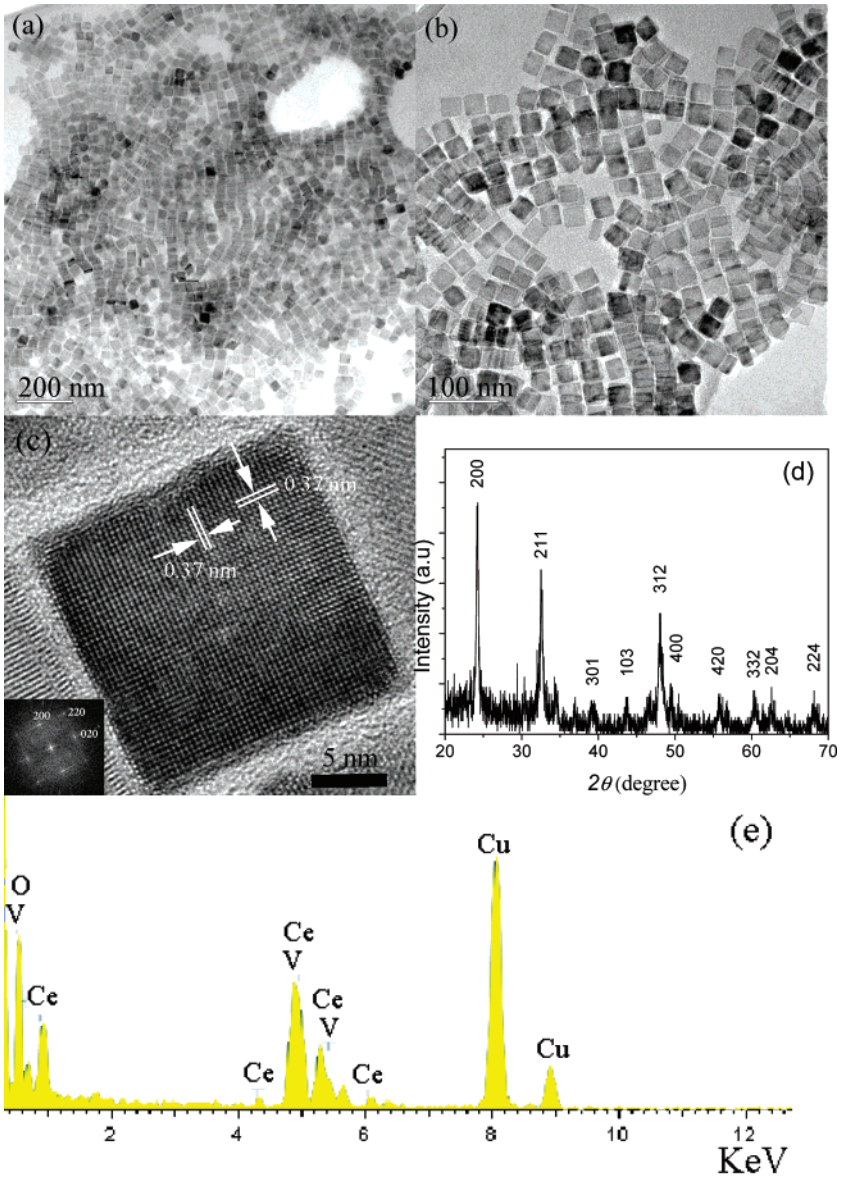

Figure 1. (a, b) TEM images of the $CeVO_4$ square-plate NCs at different magnifications; (c) HRTEM image of a single $CeVO_4$ square-plate NC and the corresponding FFT pattern (inset); (d) XRD pattern of the $CeVO_4$ square-plate NCs; (e) EDS spectrum of the $CeVO_4$ square-plate NCs.

the intensity of excitation, respectively. The excitation laser was focused onto the surface of the films (the focus length of the lens is 70 mm). The upconverted luminescence spectra from the $LnVO_4$ films were recorded by a spectrometer (Spectrapro 2500i, Acton) with liquid nitrogen cooled CCD (SPEC-10, Princeton).

Results and Discussion

Structural and Morphological Investigations. The size and morphology of the as-synthesized $CeVO_4$ NCs were characterized by TEM and HRTEM and the results are presented in Figure 1. One can see uniform squares of the $CeVO_4$ NCs at different magnifications (Figure 1a and b). Each square is estimated to be about 30 nm wide and the NCs are very regular squares with sharp facets and edges, suggesting that they are indeed single crystals. HRTEM analysis of a single square-shaped $CeVO_4$ NC in Figure 1c provided more detailed structural information. First, the HRTEM image further supports the single-crystalline nature of the NCs. Second, highly regular fringes can be seen with an interlayer distance of about 0.37 nm, which agrees well with the separation between the (200) lattice planes. Also, the single crystalline structure is mirrored in the fast Fourier transform (FFT) pattern shown in the inset of Figure 1c. According to the FFT pattern together with the HRTEM image, the four side surfaces of the square-plate NC are bounded by the {100} and {010} lattice planes, while the vertical direction is [001]. While the thickness of the NC is difficult to determine, it appears to be smaller than the lateral dimension, which is in fact why we call it "square-plate nanocrystal". The body of the square-plate was subjected to EDS analysis, confirming the exclusive composition of Ce, V, and O except for the Cu peak which can be easily attributed to arising from the copper grids (see Figure 1e). Information on the thickness of the square-plate NCs was characterized by AFM, which is estimated to be ~9 nm in the [001] direction (see Figure S1 in Supporting Information). The X-ray diffraction (XRD) pattern shown in Figure 1d further verifies the chemical composition and structure of the as-synthesized $CeVO_4$ NCs.

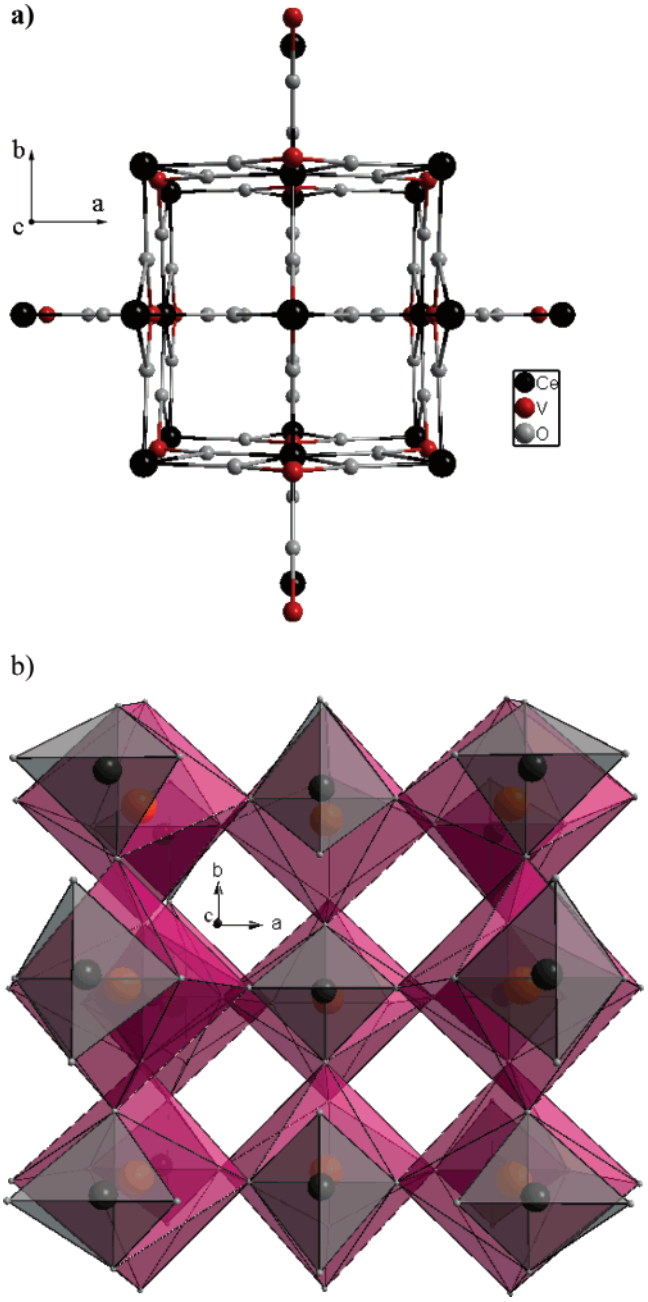

Figure 2. (a) Schematic crystal structure of the tetragonal $CeVO_4$ viewed along the *c*-axis; (b) schematic representation of the tetragonal $CeVO_4$ structure made up of VO_4 tetrahedrons and CeO_8 dodecahedrons.

One can readily index the XRD pattern to the tetragonal phase of $CeVO_4$ with lattice constants $a = 0.7399$ and $c = 0.6496$ nm (JCPDS No. 12−0757).

It is well-known that the morphology of a crystal has important effects on its physical and chemical properties, and this probably applies to NCs. In the case of our NCs, the square-plate morphology appears to be dictated by the tetragonal crystal structure of $CeVO_4$. More specifically, the as-prepared $CeVO_4$ NCs crystallize in a zircon-type tetragonal crystal system with a space group of $I4_1/amd$ as schematically depicted in Figure 2a. It consists of VO_4 tetrahedrons which along the *c*-axis are edge-linked to CeO_8 triangular dodecahedrons (Figure 2b), while along the *a*- and *b*-axes the VO_4 tetrahedrons share corners with the CeO_8 dodecahedrons. The chains comprising the alternating CeO_8 and VO_4 units extend along the *c*-crystal axis, while the CeO_8 units are edge-sharing between themselves in the *a*-*b* plane, leaving behind straight-through channels along the *c*-axis. Conceivably, the NC growth is faster along the *a*- and *b*-axes than along the *c*-axis because the framework consisting of the edge-sharing CeO_8 units is less obstructed by the VO_4 units along the *a*- and *b*-axes than along the *c*-axis, and the upshot is the formation of the square-plate $CeVO_4$ NCs as we obtained.

By adjusting the experimental condition, more specifically increasing the concentration of NaOH, a different morphology of the $CeVO_4$ NCs was obtained. As shown in Figure 3a, b, and c at different magnifications, the $CeVO_4$ NCs uniformly exhibit an interesting H-like morphology with excellent size monodispersity. Each H-shaped NC is estimated to be about 4−8 nm in the vertical direction and about 30 nm in the horizontal direction, that is, it is rather like a significantly stretched "H" letter. With the help of AFM, each H-shaped NC was found to be about 9 nm in thickness (see Figure S2 in Supporting information), which is essentially the same as for the square-plate NCs. Shown in Figure 3d is a typical HRTEM image of a single H-shaped NC with the corresponding fast Fourier transform (FFT) pattern attached in the inset. The clear, defect-free lattice fringes are evidence for the single crystallinity of the H-shaped NC. The measured fringe spacings of 0.37 and 0.489 nm are well consistent with the d-spacings of (200) and (101) planes of tetragonal $CeVO_4$, respectively. Thus the HRTEM image along with the corresponding FFT in Figure 3d proves that the H-shaped $CeVO_4$ NC extends along the ⟨100⟩ directions and its thickness is in the direction of the *c*-axis in much the same way as in the square-plate NCs described above.

To establish the generality of the synthetic method, we have extended our effort to the synthesis of NCs of the rare-earth homologues such as $NdVO_4$. As can be seen in Figure 4a and b, $NdVO_4$ NCs are also formed in the square-plate morphology. Each square is estimated to be about 30−40 nm wide. Again, by increasing the pH value in the synthesis, the H-like morphology comes into being with the $NdVO_4$ NCs, and this is clearly shown in Figure 4c and d. And the size of an individual $NdVO_4$ NC is about 6−8 nm wide and 30 nm long, much like a horizontally stretched "H" letter. The composition and crystal structure of the $NdVO_4$ NCs are also supported by EDS (Figure 4e), which shows the presence of only Nd, V, and O except for the Cu caused by the copper grid, and by XRD (Figure 4f), which validates the tetragonal phase of $NdVO_4$ with lattice constants $a = 0.7329$ and $c = 0.4356$ nm (JCPDS No. 15−0769).

Mechanisms of $LnVO_4$ NC Growth and Shape Evolution. According to the synthetic systems we adopted, the mechanism for the growth of the uniform, square-plate $CeVO_4$ and $NdVO_4$ nanocrystals can be proposed and is shown in Scheme 1. Several pivotal steps are noteworthy. First, in the primal solution, the deionized water, *n*-hexane, oleic acid, and oleylamine are expected form a reverse microemulsion, because the hydrophobic organic solvent phase (about 31 mL) is in the majority compared to the water phase (about 6 mL). The cerium(III) or neodymium(III) ions were dissolved in the water droplets of the reverse microemulsion as well as coordinated to the long ligand oleic acid (RCOOH) to form $Ln(RCOO)_x$ on the droplet surface that separates the organic and aqueous phases. Second, with the addition of VO_4^{3-}, which was also presumably dissolved in separate water droplets of the reverse microemul-

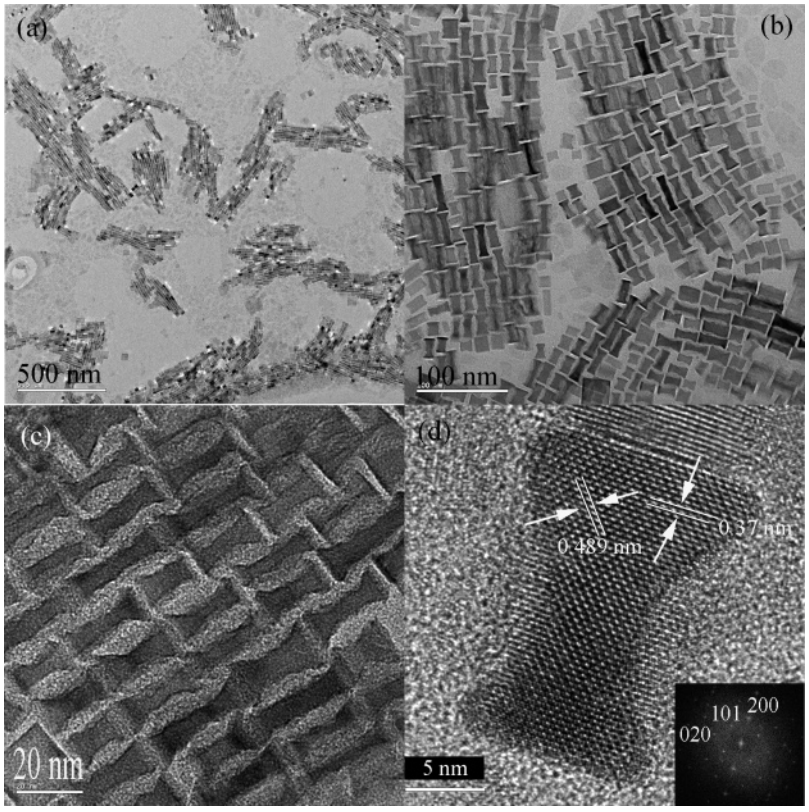

Figure 3. (a, b, c) TEM images of the $CeVO_4$ H-shaped NCs at different magnifications; (d) HRTEM image of a single $CeVO_4$ H-shaped NC and the corresponding FFT pattern (inset).

sion, nucleation and growth of $LnVO_4$ (Ln = Ce, Nd) ensued at the oil/water interfaces. Here the water droplets essentially serve as nanosized reactors, which confined the growth of the uniform $LnVO_4$ NCs, and the reaction occurs as the water droplets containing Ln^{3+} and VO_4^{3-} come in contact and exchange their interior materials. Third, our experimental results suggest that the solvo/hydrothermal conditions are critical to the formation of the high-quality square-plate NCs. Indeed, prior to the solvo/hydrothermal treatment, we did not find signs of forming NCs, and even naoparticles, in our microscopic surveys. We believe that the nucleation and growth of $LnVO_4$ are so slow under ambient condition that even regular nanoparticles have not come into shape prior to the solvo/hydrothermal treatment. However, with the solvo/hydrothermal treatment step, the $LnVO_4$ NCs are readily formed. Eventually, the surfaces of the well crystallized $LnVO_4$ NCs are strongly coordinated with and fully covered by the carboxylic groups of the oleic acids. This was confirmed by the FTIR study. A typical FTIR spectrum of the $LnVO_4$ NCs is shown in Figure 5. It is noticed that the strong absorption peak at 786 cm^{-1} agrees with the reported spectrum of a rare-earth orthovanadate, which assigned this peak to the V−O stretching vibration.[23] The $-COO^-$ asymmetric and symmetric stretching vibrations (1545 and 1438 cm^{-1}) are clearly visible (from the oleic acid).[24] Two strong peaks around 2850 and 2922 cm^{-1} can be attributed to the CH_2 and CH_3 stretching vibrations (from the oleic acid), respectively, while the broad peak at 3390 cm^{-1} is easily assigned to the O−H stretching vibration (from the oleic acid). A final remark is about the role of oleylamine used in the NC synthesis. In general, it can be consider as a cosurfactant for the stabilization of the reverse microemulsion because we found that oleylamine was indeed necessary to the synthesis of the high-quality $LnVO_4$ square-plate NCs.

It is interesting that the square-plate and H-shaped $CeVO_4$ or $NdVO_4$ NCs could be selectively synthesized by manipulating appropriate reaction parameters such as solvo/hydrothermal treatment time and pH value of the reaction mixture solution. For example, the $CeVO_4$ and $NdVO_4$ square-plate NCs were prepared by the reaction with 0.6 g NaOH for 16 h (the pH value of the solution was about 9.0 before reaction and about 6.5 after reaction), whereas the H-shaped $CeVO_4$ and $NdVO_4$ NCs were obtained with 0.9 g NaOH for 24 h (the pH value of the solution was about 10.0 before reaction and about 7.0 after reaction). The fact that a more basic solution and a longer reaction time benefit the formation of the H-shaped $CeVO_4$ and $NdVO_4$ NCs suggests that the development of the H-shape is a secondary, post-growth process. Control experiments at given initial concentrations of Ln^{3+} and NaOH and a constant temperature show that, as the reaction time increases from 10, 15, to 20 h, the H-shaped $LnVO_4$ NCs become gradually more and more regular and uniform (see Figure S3 in Supporting Information). On the basis of the experimental results above, the mechanism for evolving the H-shaped NCs is proposed and represented in Scheme 2. The main point lies in the chemical etching of the preformed square-plate NCs under the more basic condition and with a longer reaction time. On the face of it, it

(23) Amarilla, J. M.; Casal, B.; Ruiz-Hitzky, E. *Mater. Lett.* **1989**, *8*, 132−136.
(24) (a) Si, R.; Zhang, Y. W.; Zhou, H. P.; Sun, L. D.; Yan, C. H. *Chem. Mater.* **2007**, *19*, 18. (b) Park, J.; An, K.; Hwang, Y.; Park, J. G.; Noh, H. J.; Kim, J. K.; Park, J. H.; Hwang, N. M.; Hyeon, T. *Nat. Mater.* **2004**, *3*, 891.

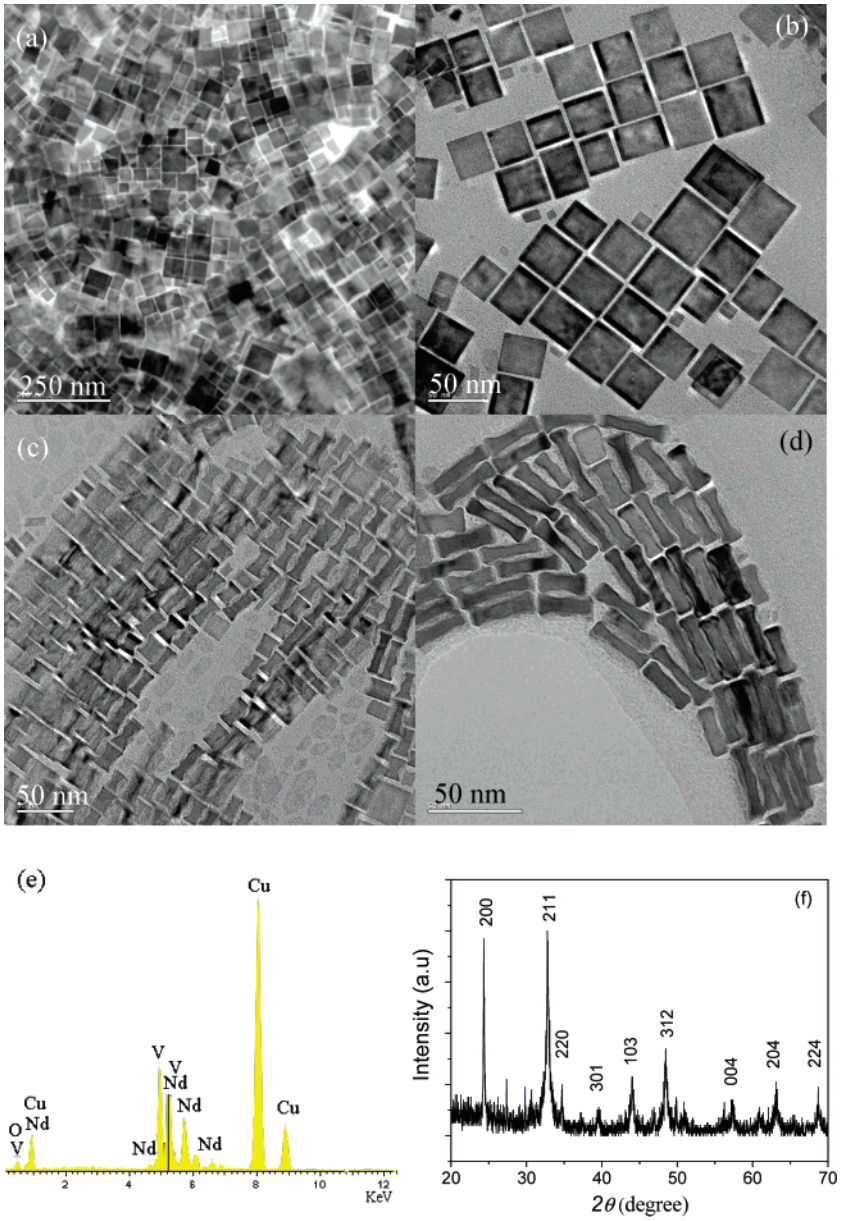

Figure 4. (a, b) TEM images of the $NdVO_4$ square-plate NCs at different magnifications; (c, d) TEM images of the $NdVO_4$ H-shaped nanocrystals at different magnifications; (e) EDS spectrum of the $NdVO_4$ square-plate NCs; (f) XRD pattern of the $NdVO_4$ square-plate NCs.

may appear that the etching should have been equally effective in both the *a*- and *b*-axes. However, once the etching jumps started, the initially attacked sites become more and more chemically active and thus preferentially etched. It seems that self-organization plays a role in the NC etching process, which ensures symmetrical etching of the opposing surfaces of the square-plate NCs, ultimately evolving into the H-shape. This is reasonable because the two opposing etched surfaces are much closer to each other and equilibrium between them, being much less limited by ion transport kinetics, is thus much more easily reached.

Upconversion Spectra of $NdVO_4$ and $CeVO_4$ NCs Films. Thick film samples were used in the measurements of upconverted luminescence, which were prepared by five runs of drop-coating on a glass slide using ethanol suspensions of the $LnVO_4$ square-plate NCs (20 mg/mL). The as-prepared thick films were dried for 3 h in air at room temperature. The thickness of the thick film was measured to be about 2 μm, and the average surface roughness reached 100 nm owing to aggregation of the NCs.

By the near-infrared excitation (λ_{exc} = 720 ~ 920 nm), $NdVO_4$ NCs thick films display three upconverted emission bands in the visible region centered at 530, 593, and 670 nm, respectively, as shown in a typical emission spectrum in Figure 6. The green emission band (~530 nm) could be attributed to the $(^2G_{9/2}-{}^4G_{11/2}) \rightarrow {}^4I_{11/2}$ and $(^4G_{7/2}-{}^4G_{9/2}) \rightarrow {}^4I_{9/2}$ transitions, whereas the orange emission (~593 nm) could be assigned to the $(^2G_{9/2}-{}^4G_{11/2}) \rightarrow {}^4I_{13/2,15/2}$ and $(^4G_{7/2}-{}^4G_{9/2}) \rightarrow {}^4I_{11/2,13/2}$ transitions, and the red emission (~670 nm) could be caused by the $(^4G_{5/2}-{}^2G_{7/2}) \rightarrow {}^4I_{9/2,11/2}$ transitions. The emission spectrum of the $NdVO_4$ NCs film is similar to that of Nd^{3+} in a KPb_2Br_5 low phonon crystal.[25]

(25) Balda, R.; Fernández, J.; Nyein, E. E.; Hömmerich, U. *Opt. Exp.* **2006**, *14*, 3993−4004.

Scheme 1. A Possible Mechanism for the Formation of the Uniform $LnVO_4$ Square-plate NCs

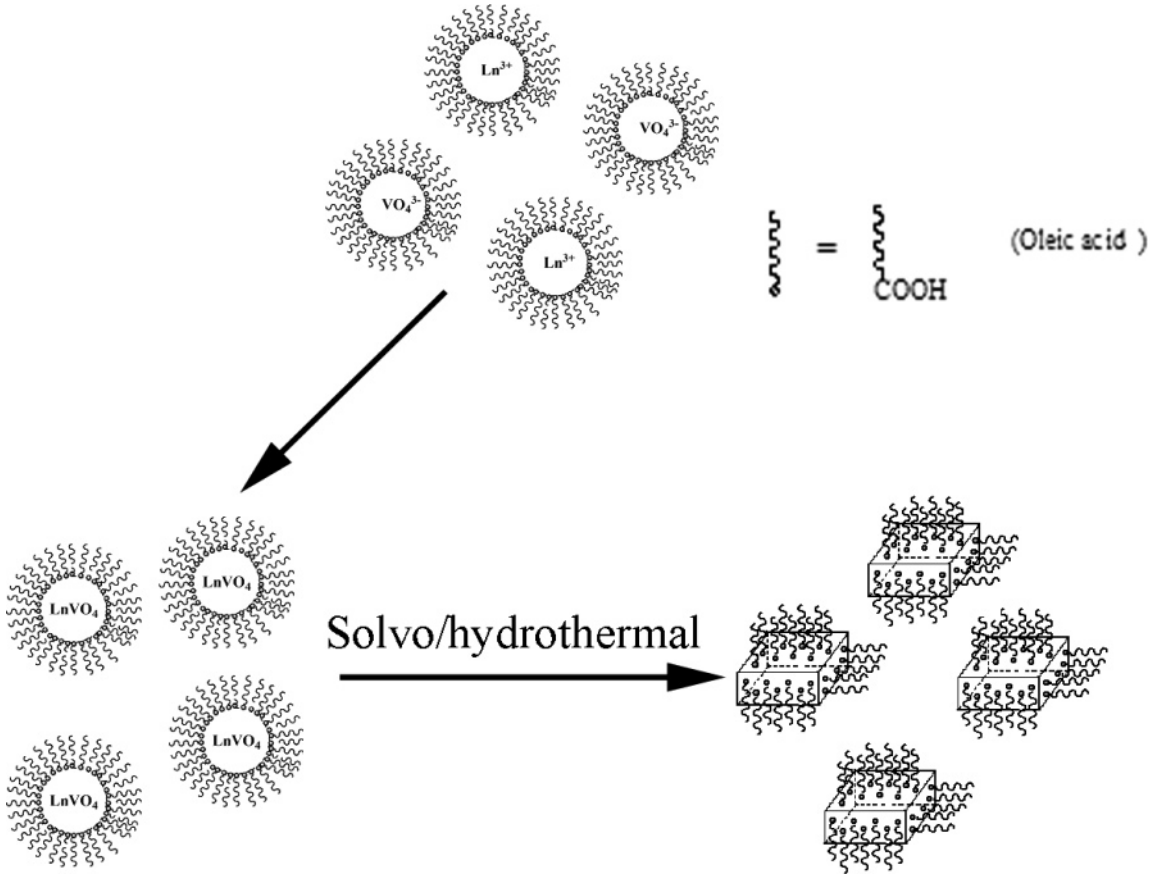

Scheme 2. A Possible Mechanism for the Shape Evolution of the $LnVO_4$ NCs from the Square-Plate to the H-like Morphology

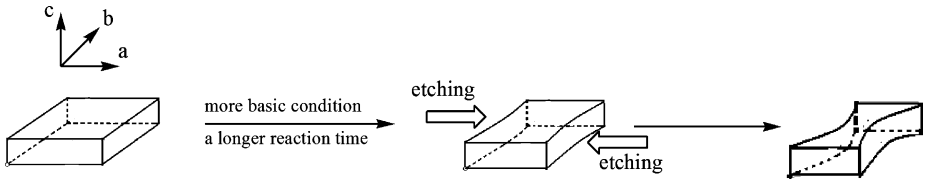

On the other hand, $CeVO_4$ NCs thick films show a broad upconverted emission band centered at 584 nm. A similar broad emission band was also observed in the one-photon ($\lambda_{exc} = 457$ nm) luminescence spectrum of Ce^{3+} in a $Y_{2.3-x}Tb_xCe_{0.05}Gd_{0.65}Al_5O_{12}$ crystal by Turos-Matysiak et al.,[26] which could be assigned to transitions from the lowest excited states arising from $5d^1$ to the ground state $4f^1$ ($^2F_{5/2}$ and $^2F_{7/2}$) of the Ce^{3+} ions. The asymmetric emission band shape is caused by the splitting of the ground state $4f^1$ due to spin−orbit interaction.[27]

Excitation Power Dependence of Upconversion Intensity of the $LnVO_4$ NCs Films. Figure 7 shows avalanche increases of the upcoverted emissions with the excitation power from the thick film samples of the $NdVO_4$ and $CeVO_4$ NCs. In the usual sense, here we refer the avalanche upconversion as a sudden increase in the emission intensity of the upcoverted photons when the excitation power is larger than a threshold value (P_c). The NCs samples were excited at $\lambda_{exc} = 800$ nm and the upconversion intensity (I_{PL}) from the $NdVO_4$ and $CeVO_4$ NCs was monitored at the emission peaks 593 and 584 nm, respectively. The avalanche slopes ($\nu_A = \partial \log I_{PL}/\partial \log P_{exc}$) reach as high as 15 and 22, respectively, for the upconverted emissions from the $NdVO_4$ and $CeVO_4$ NCs with CW excitation, and the corresponding avalanche threshold excitation powers (P_c) are about 8 and 23 mW. The much smaller P_c for the $NdVO_4$ NCs is attributed to the resonant excitation of the metastable levels $^4F_{5/2}$ of Nd^{3+}, which will be discussed later (see Figure 8). Although a number of $LnVO_4$ square-place NCs with different Ln^{3+} have been synthesized and tested for the upconversion, only those with Ln = Ce, Nd, and Y have been found to display the upconverted avalanche luminescence. The large avalanche slopes measured for the $LnVO_4$ NCs are remarkable and interesting. Such avalanche upconversions were documented for several rare-earth metal ions such as Pr^{3+}, Ho^{3+}, and Tm^{3+} doped in certain bulk optical materials,[28] which were assigned to the cross-relaxation energy transfer between the nearby fluorescent centers through the metastable intermediate levels of the rare-earth metal ions. However, the avalanche

(26) Turos-Matysiak, R.; Gryk, W.; Grinberg, M.; Lin, Y. S.; Liu, R. S. *J. Phys. Condens. Matter* **2006**, *18*, 10531−10543.
(27) You, H.; Hayakawa, T.; Nogami, M. *Appl. Phys. Lett.* **2004**, *85*, 3432−3434.

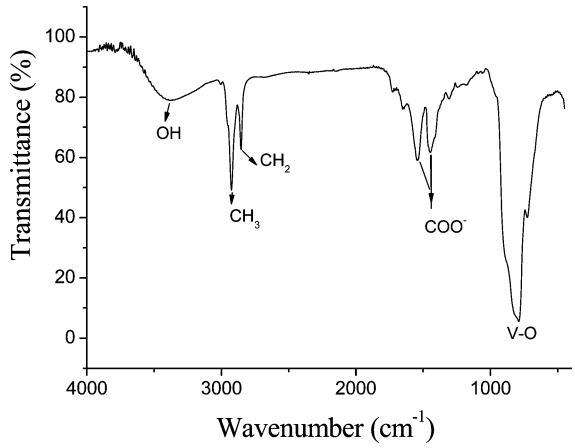

Figure 5. FTIR spectrum of the $CeVO_4$ square-plate NCs.

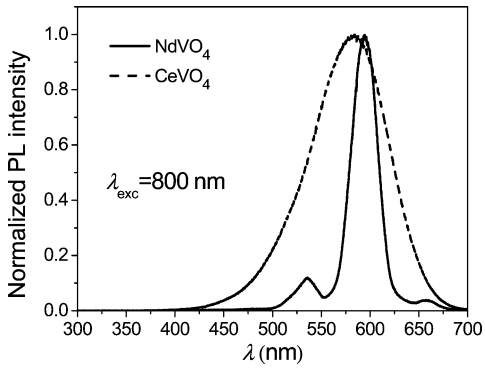

Figure 6. Upconversion spectra of the $NdVO_4$ and $CeVO_4$ NCs thick films.

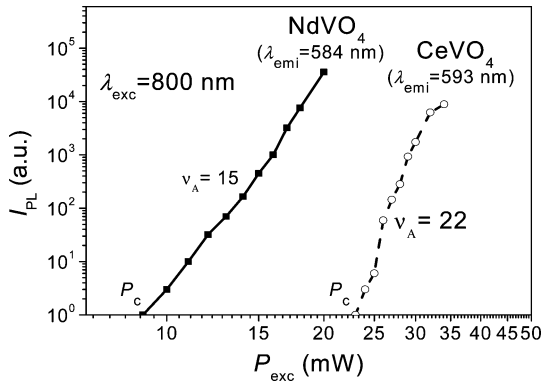

Figure 7. Excitation power dependence of upconversion intensity of the $NdVO_4$ (solid square) and $CeVO_4$ (open circle) NCs thick films, which is excited by the CW laser at $\lambda_{exc} = 800$ nm. The avalanche slopes ($\nu_A = \partial \log I_{PL}/\partial \log P_{exc}$) for the $NdVO_4$ and $CeVO_4$ NCs thick films are 15 and 22, respectively.

upconversions from the rare-earth compound NCs have not been reported until now.

To gain insight into the mechanism for the observed avalanche upconversions arising from the aggregations of the $LnVO_4$ NCs in the thick films, we undertook the same upconversion experiment on dispersed $LnVO_4$ NCs and compared the results of the $LnVO_4$ NCs with that of bulk Nd:YVO_4 reported in literature.[29] Note that from our experiments, the

(28) (a) Chivian, J. S.; Case, W. E.; Eden, D. D. *Appl. Phys. Lett.* **1979**, *35*, 124−125. (b) Lahoz, F.; Martín , I. R.; Guadalupe, V. L.; Méndez-Ramos, J.; Rodíguez, V. D.; Rodíguez-Mendoza, U. R. *Opt. Mater.* **2004**, *25*, 209−213. (c) Perlin, E. Y.; Tkachuk, A. M.; Joubert, M. F.; Moncorge, R. *Opt. Spect.* **2001**, *90*, 691−700. (d) Joubert, M. F.; Guy, S.; Jacquier, B. *Phys. Rev.* B **1993**, *48*, 10031−10037.

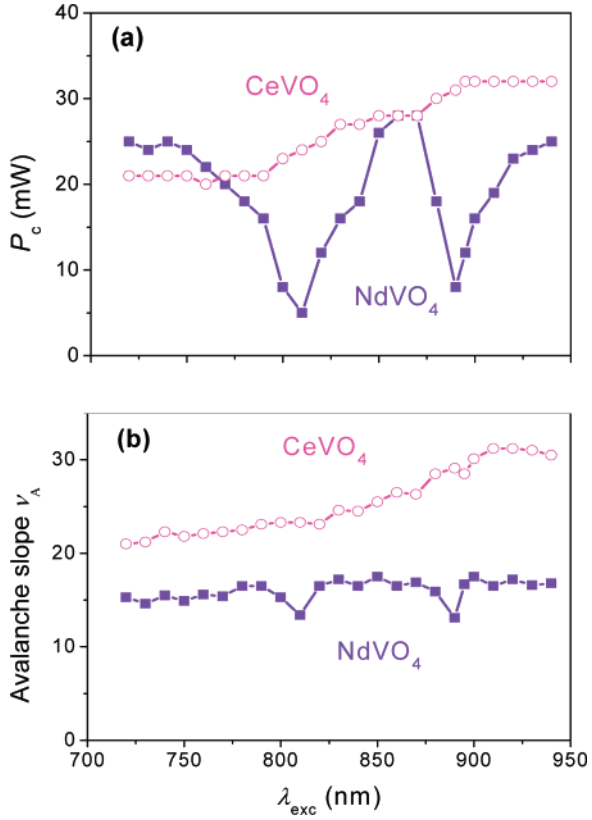

Figure 8. (a) Excitation wavelength dependence of avalanche threshold power P_c for the $NdVO_4$ (solid square) and $CeVO_4$ (open circle) NCs thick films; (b) excitation wavelength dependence of avalanche slope $\nu_A = \partial \log I_{PL}/\partial \log P_{exc}$ for the $NdVO_4$ and $CeVO_4$ NCs thick films.

avalanche upconversion properties of Nd:YVO_4 NCs films are very similar to those of the $NdVO_4$ NCs films described above. On one hand, the reported maximal value of $\partial \log I_{PL}/\partial \log P_{exc}$ for the upconversion from the Nd:YVO_4 bulk material is only about 3,[29] which is actually a three-photon induced PL process, instead of the avalanche upconversion. On the other hand, the avalanche upconversion was not observed in our experiments when the $LnVO_4$ NCs were dispersed, for example, in ethanol. This means that the avalanche cross relaxation rate dramatically decreases as the separation between the NCs increases and therefore it can be neglected within the single isolated $LnVO_4$ NCs. Furthermore, it was observed that the avalanche threshold excitation power P_c decreases sharply with the increasing thickness of the $LnVO_4$ NCs films, indicating a dramatically increasing avalanche cross relaxation rate with the increasing thickness of the NCs films. All told, our results suggest that the large extent of aggregation in the thick $LnVO_4$ NCs films have relatively large avalanche cross relaxation rates, and thus lead to the observed avalanche upconversions. It follows that the interactions between the $LnVO_4$ NCs, especially the lanthanide ions near the surface of the NCs, play a critically important role in the avalanche upconversion. Therefore, a complete avalanche upconversion mechanism for the thick $LnVO_4$ NCs films needs to take into account the proximity effects due to the NC aggregation, the size effects, including sizes of the NCs aggregates and of the NCs themselves, and the surface effects, such as the enhanced crystal fields near the surfaces of the $LnVO_4$ NCs due to the symmetry breaking.

(29) Wang, X.; Song, J.; Sun, H.; Xu, Z.; Qiu, J. *Opt. Express* **2007**, *15*, 1384−1389.

Excitation Wavelength Dependence of Avalanche Threshold Power and Avalanche Slope. Plausibly, the differences in the avalanche slope and threshold excitation power P_c between the $CeVO_4$ NCs and $NdVO_4$ NCs samples are mainly caused by the different level structures, especially the metastable levels and decay rates. Figure 8a shows variations of the avalanche threshold intensity P_c of Nd^{3+} and Ce^{3+} in VO_4^{3-} NCs with the excitation wavelength λ_{exc}. The different $P_c \sim \lambda_{exc}$ relations of the $NdVO_4$ and $CeVO_4$ NCs are caused by the different energy structures of Nd^{3+} and Ce^{3+}. The avalanche threshold intensity P_c of $NdVO_4$ NCs significantly decreases by about 80% and reaches the minima when the excitation wavelength λ_{exc} is tuned to the resonance with the metastable levels $^4F_{5/2}$ (810 nm) and $^4F_{3/2}$ (885 nm) of Nd^{3+}. This indicates that the avalanche upconversion from the $NdVO_4$ NCs is much more efficient when the metabstates $^4F_{5/2}$ and $^4F_{3/2}$ are excited resonantly. On comparing the upconversion properties of the $LnVO_4$ (Ln = Nd, Ce) NCs, one can see that the variation trends of $\nu_A \sim \lambda_{exc}$ shown in Figure 8b are very similar to those of $P_c \sim \lambda_{exc}$ shown in Figure 8a. However, the variation amplitude of $\nu_A \sim \lambda_{exc}$ is much smaller for the $NdVO_4$ NCs; the value of ν_A for the $NdVO_4$ NCs decreases by only about 18% at the resonance of the metabstates $^4F_{5/2}$ (810 nm) and $^4F_{3/2}$ (885 nm).

Conclusions

In summary, nanosized reverse microemulsion reactors coupled with a convenient and controllable solvo/hydrothermal method have been utilized for the preparation of uniform square-plate and H-shaped $LnVO_4$ NCs by simply changing the reaction time and pH. It is suggested that the square-plate nanocrystals are formed in the reverse microemulsion mediated by the solvo/hydrothermal treatments, and the H-shaped NCs are a result of etching at an extended reaction time and at a higher pH value under the solvo/hydrothermal conditions. It is expected that the nanocrystal size could also be controlled by the ratio of the aqueous and oil phases. We have uncovered an unusual avalanche upconversion phenomenon on the $LnVO_4$ NCs, and it is tentatively ascribed to an enhanced avalanche cross relaxation rate between the nearby luminescent centers. The observed avalanche upconversions are generated from the aggregation of the $CeVO_4$ and $NdVO_4$ NCs instead of the single isolated NCs, which draws attention to the importance of the proximity effects of the aggregated NCs, size effects of the NCs and NC aggregates, and surface effects of the NCs resulting in enhanced crystal fields.

We believe that the present study not only attempts to rationally design lanthanide orthovanadates NCs materials with controllable size and morphology, but also opens up new opportunities for the applications of their novel multiphoton upconverted avalanche luminescence properties. The findings in this wok will facilitate the design, fabrication and functionalization of rare-earth nanomaterials for the innovative use in optical display, ceramic laser, and chemical and biochemical sensors as well as many other areas arising from these exceptional characteristics.

Acknowledgment. We are grateful to the Research Grant Council of Hong Kong and the Hong Kong University of Science and Technology for financial supports under the grants of 604206 and RPC06/07.SC03. This work was partially supported by National Program on Key Science Research (2006CB921500) and NSFC 10534030. Thanks also go to Z. K. Zhou for the assistance in the experiments.

Supporting Information Available: Additional TEM and AFM images of the $LnVO_4$ NCs. This material is available free of charge via the Internet at http://pubs.acs.org.

JA0778141